

Unravelling the Correlation between Charge Mobility and Cocrystallization in Rod–Rod Block Copolymers for High-Performance Field-Effect Transistors

Mingjing Zhu, Shuang Pan, Yue Wang, Ping Tang, Feng Qiu, Zhiqun Lin,* and Juan Peng*

Abstract: Cocrystallization involving two or more components aggregating into cocrystals allows the preparation of materials with markedly improved charge mobility. This approach however, is little explored in all-conjugated block copolymers (BCPs). Herein, we report the first investigation into the correlation between cocrystals and charge mobility in a series of new all-conjugated BCPs: poly(3-butylthiophene)-*b*-poly(3-hexylselenophene) (P3BT-*b*-P3HS) for high-performance field-effect transistors. These rationally synthesized rod–rod BCPs self-assemble into cocrystals with high charge mobilities. Upon one-step thermal annealing, their charge mobilities decrease slightly despite their increased crystallinities. After two-step thermal annealing, P3BT-*b*-P3HS (P3BT/P3HS = 2:1) and (1:1) cocrystals disappear and phase separation occurs, leading to greatly decreased charge mobilities. In contrast, P3BT-*b*-P3HS (1:2) retains its cocrystalline structure and its charge mobility.

Organic field-effect transistors (OFETs) containing π -conjugated small molecules and polymers as the active semiconducting layer have garnered considerable attention owing to their attractive low-cost, light-weight, flexible and solution-processable attributes.^[1] To date, most of reported OFETs are based on single-component materials with their own intrinsic properties.^[2] Recently, a cocrystallization strategy for OFETs has emerged by aggregating two or more dissimilar small molecules into cocrystals, exhibiting versatile, multifunctional properties (e.g., ambipolar transport behavior with balanced electron and hole field-effect mobilities).^[3–5] However, it is notable that all OFETs based on organic cocrystals are largely limited to small molecules. Surprisingly, the use of conjugated polymer cocrystals for OFETs has not yet been reported. Compared with small molecular cocrystals produced through non-covalent interactions,^[3–5] it remains challenging to form polymer cocrystals as three requirements

need to be fulfilled simultaneously, that is, structural similarity, comparable potential energies, and crystallization kinetics.^[6] As a result, to date very few polymer cocrystal pairs have ever been demonstrated.^[7–10] As conjugated polymers are particularly advantageous for large-area, flexible electronics, and more importantly their cocrystals may display intriguing new structures, properties, and functionalities without complicated synthesis, there is a vital need and opportunity to develop conjugated polymer cocrystals for high-performance OFETs.

All-conjugated rod–rod block copolymers (BCPs) represent an emerging class of functional materials as they possess fascinating self-assembly properties of BCPs and optoelectronic properties of conjugated constituents.^[11] Among rod-rod BCPs, poly(3-alkylthiophene)s (P3ATs)-based BCPs have gained immense interest^[8–10,12–14] and several P3ATs-based BCPs are found to have cocrystalline structures including poly(3-butylthiophene)-*b*-poly(3-hexylthiophene) (P3BT-*b*-P3HT)^[9] and poly(2,5-dihexyloxy-*p*-phenylene)-*b*-poly(3-(2-ethylhexyl)thiophene) (PPP-*b*-P3EHT).^[10] Notably, these cocrystals carry some main disadvantages, such as similar electronic properties due to the same conjugated backbone^[9] or relatively low crystallinity,^[10] thus preventing them from being employed for high-performance OFETs. Clearly, to overcome the issues noted above, it is highly desirable to develop new all-conjugated BCPs possessing two disparate π -conjugated blocks yet highly crystalline.

Compared to the heavily studied P3ATs, their analogue poly(3-alkylselenophene)s (P3ASs) are much less investigated.^[15,16] Selenium atom substitution carries advantages over P3ATs, such as stronger intermolecular interaction, narrower band gap and improved planarity, thereby favoring charge transport.^[16] However, the stronger Se–Se interaction also reduces the polymer solubility and the larger Se atoms lead to the increased π – π stacking distance. It is noteworthy that P3ATs and P3ASs have similar molecular structures and carry respective excellent optoelectronic properties, rod–rod BCPs composed of polythiophene and polyselenophene blocks may offer great potential to form cocrystals and exhibit enhanced optoelectronic properties over the two respective constituents.

Herein, we report, for the first time, the judicious design and synthesis of a series of new P3BT-*b*-P3HS BCPs and manifest a strong correlation between cocrystallization of BCPs and their high field-effect mobilities. As-cast P3BT-*b*-P3HS thin films are found to yield cocrystals with an edge-on orientation and exhibit over an order of magnitude higher charge mobility than that of the corresponding homopolymers. After one-step thermal annealing, charge mobilities of

[*] M. Zhu, S. Pan, Y. Wang, Prof. P. Tang, Prof. F. Qiu, Prof. J. Peng
State Key Laboratory of Molecular Engineering of Polymers
Department of Macromolecular Science
Fudan University
Shanghai 200433 (China)
E-mail: juanpeng@fudan.edu.cn

S. Pan, Prof. Z. Lin
School of Materials Science and Engineering
Georgia Institute of Technology
Atlanta, GA 30332 (USA)
E-mail: zhiqun.lin@mse.gatech.edu

Supporting information and the ORCID identification number(s) for the author(s) of this article can be found under:
<https://doi.org/10.1002/anie.201804585>.

P3BT-*b*-P3HS cocrystal films decrease slightly despite their enhanced crystallinities. The increase in crystallite sizes and the improved long-range orders along the lamellar packing direction (i.e., film thickness direction; resulting from non-conjugated alkyl side chains) instead of along the π - π stacking direction (i.e., lateral direction, that is, conjugated backbone stacking direction) are found, which may account for the slightly decreased charge mobilities. Interestingly, after two-step thermal annealing, the cocrystals of P3BT-*b*-P3HS (both 2:1 and 1:1) disappear and transition into individual P3BT and P3HS crystal domains, leading to largely decreased charge mobility. On the other hand, P3BT-*b*-P3HS (1:2) remains cocrystalline and has similar charge mobility to that of the one-step annealing sample. These results further corroborate that the cocrystalline structure of P3BT-*b*-P3HS BCPs correlates positively with their charge transport properties. On the basis of this work, the ability of easily forming cocrystals in all-conjugated BCPs with markedly enhanced charge mobility without the need of post-thermal or solvent annealing may enable them for a wide range of potential applications in optoelectronic materials and devices.

Three P3BT-*b*-P3HS BCPs with varied P3BT/P3HS block ratios (P3BT/P3HS = 2:1, 1:1, and 1:2) and molecular weights ranging from 19600 to 21800 with a narrow polydispersity index (PDI) of 1.13–1.21 were synthesized by Grignard metathesis (GRIM) polymerization (Scheme S1 in the Supporting Information).^[17] For control experiments, homopolymers of P3BT and P3HS, as well as statistical copolymer of P3BT-*s*-P3HS were also synthesized. Detailed synthetic procedures, polymer characterizations (¹H NMR spectroscopy and gel permeation chromatography; GPC), and a summary of their molecular weights are in the Supporting Information (Figures S1 and S2, Table S1).

The molecular structure and frontier orbital distributions of thiophene and selenophene were calculated via density functional theory (DFT; Figure S3). The quinoid coefficient f is used to measure the relative importance of the aromatic character with respect to the quinoid character of the structure.^[18] The thiophene and selenophene oligomers show a f of 1.028 and 1.022, respectively (Figure S3a), suggesting a greater quinoid-like structure and higher planarity of selenophene oligomer. Moreover, the dihedral angles of thiophene–thiophene units and selenophene–selenophene units in the copolymer chain were calculated to be 22.3° and 0.3°, respectively (Figure S3b), indicating the more planar selenophene backbone than the thiophene backbone. Clearly, the high planarity of

polymer chain imparts good charge transport. Figure S3c depicts that the calculated highest occupied molecular orbital (HOMO) and lowest unoccupied molecular orbital (LUMO) distribution contours are more occupied by the selenophene block, signifying a greater effect of the selenophene block on determining the band gap of BCPs.^[19] By calculation, the theoretical E_g of thiophene-selenophene BCP, selenophene and thiophene oligomer is 1.75 eV, 1.73 eV and 1.97 eV, respectively (Table S2). This result suggests that theoretical E_g of thiophene-selenophene BCP is close to that of selenophene oligomer. The actual HOMO and LUMO energy levels of three P3BT-*b*-P3HS BCPs were measured by cyclic voltammetry (CV; Figure S4) and UV/Vis absorption spectroscopy in solid thin-film state (Figure S5), and summarized in Table S2 and Figure S6. The results suggest that the three P3BT-*b*-P3HS BCPs exhibit the E_g (1.70–1.71 eV), close to that of P3HS homopolymer (1.68 eV) and much lower than that of P3BT homopolymer (1.90 eV), which is in good agreement with the theoretical E_g , demonstrating the profound influence of selenophene block on the E_g of BCPs.

Molecular packing and crystalline orientation of three as-cast P3BT-*b*-P3HS thin films with varied P3BT/P3HS block ratios were scrutinized by 2D synchrotron grazing-incidence X-ray diffraction (2D-GIXRD; Figure 1). Figure 1a depicts the schematic of the synchrotron GIXRD measurement. All three as-cast P3BT-*b*-P3HS samples exhibit only one single (100) diffraction peak at q_z of 4.72 nm⁻¹ (d_{100} = 13.31 Å; P3BT/P3HS = 2:1), 4.48 nm⁻¹ (d_{100} = 14.02 Å; P3BT/P3HS = 1:1), and 4.24 nm⁻¹ (d_{100} = 14.81 Å; P3BT/P3HS = 1:2), respectively (Figure 1b,c). Their π - π stacking distances are 3.79, 3.81, and 3.86 Å with the scattering vectors $q_{x,y}$ of 16.57, 16.48, and 16.26 nm⁻¹, respectively. It suggests all three BCP samples form cocrystallization in the edge-on orientation with the direction of π - π stacking and the layers of alkyl side chains parallel and perpendicular to the substrate, respec-

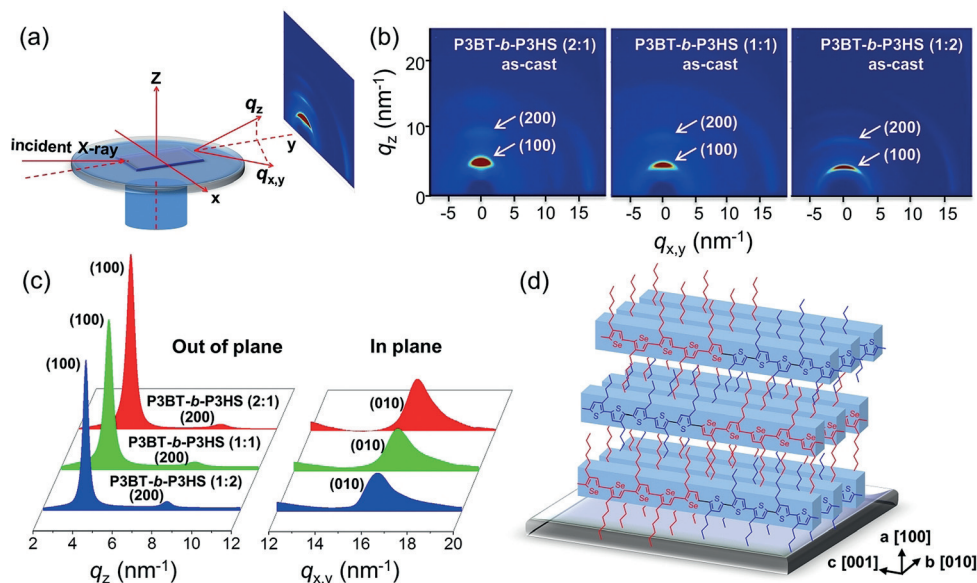


Figure 1. a) Schematic illustration of 2D synchrotron GIXRD measurement on samples. b) 2D-GIXRD patterns of three as-cast P3BT-*b*-P3HS thin films. c) 1D GIXRD profiles along the out-of-plane (q_z) and in-plane ($q_{x,y}$) directions from the corresponding 2D-GIXRD patterns in (b). d) Schematic representation of chain arrangements in P3BT-*b*-P3HS cocrystals.

tively. Both d_{100} and d_{010} of BCPs are between those of P3BT ($d_{100} = 12.5 \text{ \AA}$; $d_{010} = 3.77 \text{ \AA}$) and P3HS ($d_{100} = 15.4 \text{ \AA}$; $d_{010} = 3.91 \text{ \AA}$) homopolymers and gradually increase with the increased P3HS content as the P3HS block has larger d_{100} and d_{010} spacing (Figure S7). In contrast, the P3BT/P3HS blend shows two (100) diffraction peaks at q_z of 4.98 and 4.15 nm^{-1} , implying that P3BT and P3HS form two individual crystals in the blend (Figure S7). By DSC measurement, a single endothermic peak at 278°C , 266°C and 212°C was observed for P3BT-*b*-P3HS (2:1), (1:1), and (1:2), respectively, while two endothermic peaks at 280°C and 213°C can be seen in the P3BT/P3HS blend (Figure S8). These results agree well with the 2D-GIXRD studies and further confirm the formation of cocrystals in as-cast P3BT-*b*-P3HS BCPs. The P3BT-*b*-P3HS cocrystals are quite stable in ambient condition over a long period of time. Figure 1d depicts the possible chain arrangement in an edge-on orientation for P3BT-*b*-P3HS cocrystals, where the hexyl and butyl side chains in the P3HS and P3BT blocks, respectively, of BCPs compromise to yield a balanced d_{100} -spacing by adjusting their conformations.

To unravel the correlation between the crystalline structures of P3BT-*b*-P3HS and their charge transport properties, top-contact bottom-gate OFET devices were fabricated. The transfer and output curves of P3BT-*b*-P3HS cocrystal films and control samples of P3BT, P3HS, P3BT/P3HS blend and P3BT-*s*-P3HS are shown in Figure 2 and Figure S9, and their mobilities are summarized in Table S1. As-cast P3BT-*b*-P3HS cocrystal films without any post-thermal or solvent vapor treatment exhibited the average charge mobilities of $0.03\text{--}0.04 \text{ cm}^2 \text{ V}^{-1} \text{ s}^{-1}$. The highest charge mobility of $0.045 \text{ cm}^2 \text{ V}^{-1} \text{ s}^{-1}$ was found in P3BT-*b*-P3HS (2:1), which is over one order of magnitude higher than the control samples ($5.0 \times 10^{-4} \text{ cm}^2 \text{ V}^{-1} \text{ s}^{-1}$ for P3BT; $2.0 \times 10^{-3} \text{ cm}^2 \text{ V}^{-1} \text{ s}^{-1}$ for P3HS; $1.2 \times 10^{-3} \text{ cm}^2 \text{ V}^{-1} \text{ s}^{-1}$ for P3BT/P3HS blend) and the P3BT-*s*-P3HS statistical copolymer ($6.0 \times 10^{-3} \text{ cm}^2 \text{ V}^{-1} \text{ s}^{-1}$). To our knowledge, this is the highest reported charge mobility based on poly(3-alkylthiophene)s (P3ATs) or poly(3-alkylselenophene)s (P3ASs) thin films via simple spin-coating, dispensing with the need for additional treatments.^[20–23] It is interesting to note that charge mobilities of as-cast P3BT-*b*-P3HS thin films are comparable to the reported thermal-annealed P3ATs ($0.01\text{--}0.10 \text{ cm}^2 \text{ V}^{-1} \text{ s}^{-1}$)^[22] and P3ASs ($0.02\text{--}0.04 \text{ cm}^2 \text{ V}^{-1} \text{ s}^{-1}$).^[15] More comparison of charge mobilities obtained in this work with other reported polythiophene or polyselenophene-based systems is provided in Figure S10.

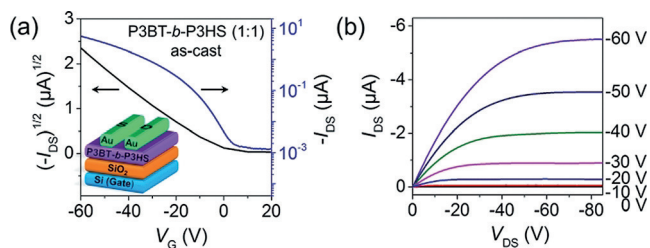


Figure 2. a) Transfer and b) output curves of OFETs fabricated using as-cast P3BT-*b*-P3HS (P3BT/P3HS = 1:1) cocrystal film. $V_{DS} = -60 \text{ V}$. Inset: schematic illustration of OFET device structure.

These as-cast P3BT-*b*-P3HS cocrystal films show nanowire morphology and a relatively smooth surface with the root-mean-square roughness of 3.43 nm, 2.14 nm, and 1.28 nm in P3BT-*b*-P3HS (2:1), (1:1), and (1:2), respectively, by atomic force microscopy (AFM; Figure S11). Taken the GIXRD and AFM results together, it is clear that as-cast P3BT-*b*-P3HS BCPs self-assemble into ordered cocrystalline structure that renders the efficient charge transport pathway, thereby resulting in high charge mobilities.

Thermal annealing has been widely used to manipulate the crystalline structure and improve the ordering of molecular packing of conjugated polymers.^[24] In this context, we carried out two different thermal annealing strategies, that is, one-step and two-step thermal annealing, to further correlate different crystalline structures of P3BT-*b*-P3HS with their charge transport properties. For one-step thermal annealing, it was conducted at 150°C to improve the ordering of molecular packing of P3BT-*b*-P3HS. For two-step thermal annealing, P3BT-*b*-P3HS cocrystal films were first annealed at the temperature near their melting points to ensure the copolymer chain mobility and escaping from the cocrystals as well as facilitate the isothermal crystallization of one block of BCP first while retaining the second block in the molten state. Subsequently, isothermal crystallization of the second block of BCP at 150°C was followed. It is worth noting that such an annealing strategy was motivated by the notion that if two blocks in cocrystals are endowed with greatly different chain mobilities, the crystalline structure of P3BT-*b*-P3HS BCPs may be tailored from cocrystals to individual crystals of each block, and thus phase separation of P3BT-*b*-P3HS BCPs may happen.

In one-step thermal annealing described above, P3BT-*b*-P3HS films with varied block ratios showed only one more intense and sharper (100) reflections compared to as-cast samples, indicating that cocrystals still exist yet with increased crystallinity (Figure 3a). The control samples including P3BT, P3HS, P3BT/P3HS blend, and P3BT-*s*-P3HS also exhibited increased crystallinity after 150°C thermal treatment (Figure S12).

In contrast, two-step thermal annealing yielded intriguing results. The melting points of three P3BT-*b*-P3HS (2:1), (1:1), and (1:2) are 278 , 266 , 212°C , respectively (Figure S8). These three cocrystal films were thermal-annealed at 260°C , 230°C , and 200°C for 10 min, respectively, followed by annealing at 150°C for 10 min. For P3BT-*b*-P3HS (2:1) and (1:1) thin films, the previous single (100) diffraction peak at q_z of 4.72 nm^{-1} and 4.48 nm^{-1} , respectively, disappeared. The two (100) diffraction peaks were clearly observed at q_z of 4.79 nm^{-1} and 4.24 nm^{-1} for P3BT-*b*-P3HS (2:1) and q_z of 4.83 nm^{-1} and 4.19 nm^{-1} for P3BT-*b*-P3HS (1:1), respectively, which can be ascribed to the crystallization of individual P3BT and P3HS blocks (Figure 3c). This signifies that P3BT-*b*-P3HS cocrystals were destroyed, and the phase separation of P3BT-*b*-P3HS (2:1) and (1:1) occurred. Notably, single (100) diffraction peak is persisted in P3BT-*b*-P3HS (1:2) thin film, suggesting that the retention of cocrystalline structure after two-step thermal annealing (Figure 3c). The different 2D-GIXRD results of P3BT-*b*-P3HS BCPs after two-step thermal annealing can be rationalized as follows. To identify the

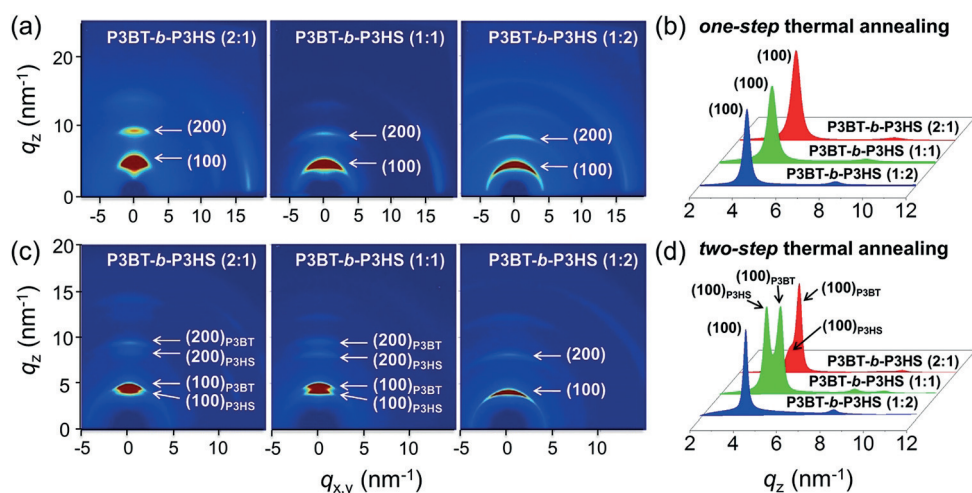


Figure 3. 2D-GIXRD patterns of three P3BT-*b*-P3HS thin films after a) one-step thermal annealing, and c) two-step thermal annealing. b) and d) 1D GIXRD profiles along the out-of-plane (q_z) direction from the corresponding 2D-GIXRD patterns in (a) and (c), respectively.

melting points of P3BT and P3HS blocks in three BCPs, three P3BT ($M_n = 12.0, 9.0,$ and 5.5 KDa) and three P3HS ($M_n = 16.0, 13.0,$ and 9.0 KDa) homopolymers were synthesized with their molecular weights close to the constituent P3BT and P3HS blocks in BCPs ($M_{n,P3BT} = 12.0$ KDa and $M_{n,P3HS} = 7.6$ KDa in P3BT-*b*-P3HS (2:1); $M_{n,P3BT} = 8.5$ KDa and $M_{n,P3HS} = 13.3$ KDa in P3BT-*b*-P3HS (1:1); $M_{n,P3BT} = 5.3$ KDa and $M_{n,P3HS} = 16.0$ KDa in P3BT-*b*-P3HS (1:2)). The melting points of these P3BT and P3HS homopolymers were also measured by DSC (Figure S13) and summarized in Table S3. For P3BT-*b*-P3HS (2:1) and (1:1), during the first-step annealing at 260°C and 230°C , the P3HS blocks with their melting points of approximately 187°C and 202°C , are destroyed in the cocrystal and melted into coil-like chains. While the P3BT blocks remain rod-like chains owing to their higher melting points (ca. 275°C and 267°C for the P3BT block in P3BT-*b*-P3HS (2:1) and (1:1), respectively) and crystallized to form the P3BT crystalline domain solely. Subsequently, P3HS chains crystallize during the second-step annealing at 150°C to complete the transition from cocrystals to two individual P3BT and P3HS crystals. However, for P3BT-*b*-P3HS (1:2), the melting point of P3BT decreases to approximately 218°C (Figure S13), which is very close to the melting point of P3HS block ($M_{n,P3HS} = 16.0$ KDa, $T_m = 210^\circ\text{C}$). Therefore, P3BT and P3HS blocks may have similar chain mobility during the first-step (200°C) and the second-step annealing (150°C) processes, thus maintaining the cocrystalline structure. The corresponding 1D GIXRD profiles of three BCPs after one-step and two-step thermal annealing along the out-of-plane (q_z) direction are presented in Figure 3b, d.

The charge transport properties of three P3BT-*b*-P3HS thin films after different thermal annealing pathways were compared (Figure 4 and Figure S14). After one-step thermal annealing, charge mobilities of control samples including P3BT, P3HS, P3BT/P3HS blend and P3BT-*s*-P3HS markedly increased to $0.008, 0.006, 0.010,$ and 0.034 $\text{cm}^2\text{V}^{-1}\text{s}^{-1}$, respectively, while surprisingly three P3BT-*b*-P3HS BCPs displayed

slightly decreased mobilities of $0.023\text{--}0.031$ $\text{cm}^2\text{V}^{-1}\text{s}^{-1}$ (Table S1). This indicates thermal annealing at 150°C does not exert a favorable influence on charge mobilities of P3BT-*b*-P3HS cocrystals.

To uncover the possible reasons as to why P3BT-*b*-P3HS cocrystal films have different performance from control samples, we performed a more detailed analysis from the molecular packing viewpoint by calculating the number of lamellar packing layers along the (100) direction (N_{100}) and the number of π - π stacking layers along the (010) direction (N_{010}) (Table S4).^[19] A detailed

explanation and calculation of each individual parameter can be found in the Supporting Information. As shown in Table S4, for control samples, the increased number of lamellar packing layers ($\Delta N_{100} = N_{100,150^\circ\text{C}} - N_{100,\text{as-cast}}$) and π - π stacking layers ($\Delta N_{010} = N_{010,150^\circ\text{C}} - N_{010,\text{as-cast}}$) of P3BT, P3HS, P3BT/P3HS blend and P3BT-*s*-P3HS are 3.8, 3.9, 1.8/2.6, 3.6 for ΔN_{100} , and 3.6, 3.2, 2.1/2.5, 3.2 for ΔN_{010} , respectively. ΔN_{100} and ΔN_{010} at these two directions are roughly equal in control samples, indicating no selective growth of both the crystalline size and long-range order during the one-step thermal annealing. This promotes the increase of charge mobility. However, for P3BT-*b*-P3HS BCPs, ΔN_{100} in P3BT-*b*-P3HS (2:1), (1:1), and (1:2) are 2.7, 2.9, and 2.7, respectively, which are more than two times ΔN_{010} (1.3, 1.1, and 1.1, respectively). Clearly, this implies that the crystalline size and long-range order preferentially increase along the (100) direction (i.e., alkyl side chain direction), which does not contribute to the increase of charge mobility because charge transport occurs primarily along the polymer backbone (i.e.,

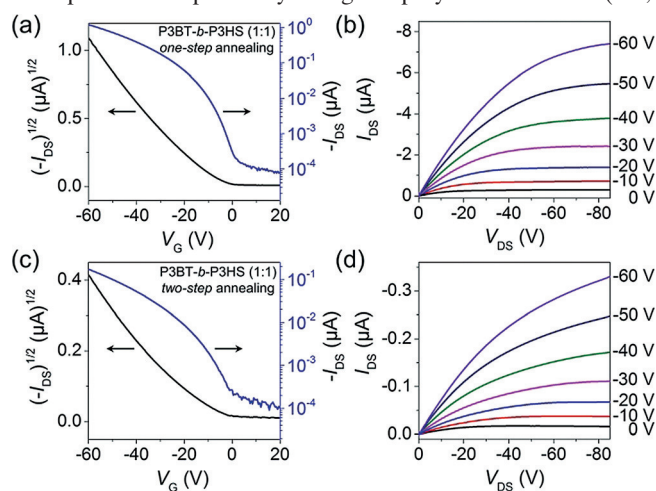


Figure 4. a), c) Transfer and b), d) output curves of OFETs fabricated using P3BT-*b*-P3HS (P3BT/P3HS = 1:1) thin film after a), b) one-step thermal annealing and c), d) two-step thermal annealing. $V_{DS} = -60$ V.

(001) direction) and π - π stacking (i.e., (010) direction) directions (Figure 1d). Thus, despite the increase of crystallinity in P3BT-*b*-P3HS cocrystals after one-step thermal annealing, the slight decrease of their charge mobilities can be understood on the basis of thorough GIXRD analysis described above.

For charge transport properties of P3BT-*b*-P3HS thin films after two-step thermal annealing, P3BT-*b*-P3HS (2:1) and (1:1) demonstrated greatly decreased charge mobility to $10^{-3} \text{ cm}^2 \text{ V}^{-1} \text{ s}^{-1}$. However, P3BT-*b*-P3HS (1:2) maintained a charge mobility up to $0.025 \text{ cm}^2 \text{ V}^{-1} \text{ s}^{-1}$. As discussed above, the cocrystals were destroyed in P3BT-*b*-P3HS (2:1) and (1:1) while remaining in P3BT-*b*-P3HS (1:2) after two-step thermal annealing. Thus, these charge mobility results further confirm that the P3BT and P3HS cocrystalline structure is the key to good charge transport property. It is interesting to note that P3BT-*b*-P3HS (2:1) and (1:1) thin films showed two phase-separated nanostructures after two-step thermal annealing (Figure S15) compared to their morphologies obtained from as-cast and after one-step thermal annealing. On the basis of the above analysis, the structural models of P3BT-*b*-P3HS (2:1) and (1:1) before and after one-step or two-step thermal annealing can be depicted in Figure S16.

In summary, we have rationally designed and synthesized a series of P3BT-*b*-P3HS BCPs with tunable block ratios, and scrutinized the strong correlation between their crystalline structures and charge transport properties. Importantly, as-cast BCPs form cocrystals and exhibit the highest charge mobility of $0.045 \text{ cm}^2 \text{ V}^{-1} \text{ s}^{-1}$, dispensing with the need for post-thermal and solvent vapor treatment. The one-step thermal annealing increases the crystallinities of P3BT-*b*-P3HS cocrystal films while their charge mobilities decrease slightly. Interestingly, upon two-step thermal annealing, the cocrystals originally existed in P3BT-*b*-P3HS (2:1) and (1:1) disappear, and consequently their charge mobilities decrease significantly. However, the cocrystals remain in P3BT-*b*-P3HS (1:2) and thus keep the similar charge mobility to one-step thermal annealing counterpart. This study elucidates that the existence of cocrystals is of key importance for high charge mobility of P3BT-*b*-P3HS. As such, facile synthesis and attainable high charge mobility in the absence of post-annealing may make this class of all-conjugated BCPs promising materials for large-scale manufacturing of low-cost OFET and other devices.

Acknowledgements

This work was financially supported by the National Natural Science Foundation of China (Grant NOs. 21674024, 21320102005) and Ministry of Science and Technology of China (2016YFA0203301). Z.L. acknowledges the Senior Visiting Scholarship of State Key Laboratory, Fudan University. We gratefully acknowledge the support from Shanghai Synchrotron Radiation Facility of China for using the BL14B1 and BL16B1 beamlines.

Conflict of interest

The authors declare no conflict of interest.

Keywords: cocrystallization · copolymers · organic field-effect transistors (OFETs) · polyselenophenes · rod-rod block copolymer

How to cite: *Angew. Chem. Int. Ed.* **2018**, *57*, 8644–8648
Angew. Chem. **2018**, *130*, 8780–8784

- [1] C. L. Wang, H. L. Dong, W. P. Hu, Y. Q. Liu, D. B. Zhu, *Chem. Rev.* **2012**, *112*, 2208–2267.
- [2] L. Ying, F. Huang, G. C. Bazan, *Nat. Commun.* **2017**, *8*, 14047.
- [3] L. Y. Zhu, Y. P. Yi, Y. Li, E.-J. Kim, V. Coropceanu, J.-L. Brédas, *J. Am. Chem. Soc.* **2012**, *134*, 2340–2347.
- [4] J. Zhang, J. H. Tan, Z. Y. Ma, W. Xu, G. Y. Zhao, H. Geng, C. A. Di, W. P. Hu, Z. G. Shuai, K. Singh, D. B. Zhu, *J. Am. Chem. Soc.* **2013**, *135*, 558–561.
- [5] H. T. Black, D. F. Perepichka, *Angew. Chem. Int. Ed.* **2014**, *53*, 2138–2142; *Angew. Chem.* **2014**, *126*, 2170–2174.
- [6] J. Datta, A. K. Nandi, *Polymer* **1994**, *35*, 4804–4812.
- [7] S. Pal, A. K. Nandi, *Macromolecules* **2003**, *36*, 8426–8432.
- [8] C.-C. Ho, Y.-C. Liu, S.-H. Lin, W.-F. Su, *Macromolecules* **2012**, *45*, 813–820.
- [9] J. Ge, M. He, F. Qiu, Y. L. Yang, *Macromolecules* **2010**, *43*, 6422–6428.
- [10] Y.-H. Lee, W.-C. Chen, Y.-L. Yang, C.-J. Chiang, T. Yokozawa, C.-A. Dai, *Nanoscale* **2014**, *6*, 5208–5216.
- [11] A. Yassar, L. Miozzo, R. Girona, G. Horowitz, *Prog. Polym. Sci.* **2013**, *38*, 791–844.
- [12] X. B. Yang, J. Ge, M. He, Z. Ye, X. F. Liu, J. Peng, F. Qiu, *Macromolecules* **2016**, *49*, 287–297.
- [13] M. He, W. Han, J. Ge, Y. L. Yang, F. Qiu, Z. Q. Lin, *Energy Environ. Sci.* **2011**, *4*, 2894–2904.
- [14] D. Gao, J. Hollinger, D. S. Seferos, *ACS Nano* **2012**, *6*, 7114–7121.
- [15] M. Heeney, W. M. Zhang, D. J. Crouch, M. L. Chabinye, S. Gordeyev, R. Hamilton, S. J. Higgins, I. McCulloch, P. J. Skabara, D. Sparrowe, S. Tierney, *Chem. Commun.* **2007**, 5061–5063.
- [16] A. Patra, M. Bendikov, *J. Mater. Chem.* **2010**, *20*, 422–433.
- [17] A. Yokoyama, R. Miyakoshi, T. Yokozawa, *Macromolecules* **2004**, *37*, 1169–1171.
- [18] A. Omrani, H. Sabzyan, *J. Phys. Chem. A* **2005**, *109*, 8874–8879.
- [19] Y. Wang, T. Hasegawa, H. Matsumoto, T. Mori, T. Michinobu, *Adv. Funct. Mater.* **2017**, *27*, 1604608.
- [20] Y. Zhang, K. Tajima, K. Hashimoto, *Synth. Met.* **2011**, *161*, 225–228.
- [21] C.-C. Chueh, T. Higashihara, J.-H. Tsai, M. Ueda, W.-C. Chen, *Org. Electron.* **2009**, *10*, 1541–1548.
- [22] A. Zen, J. Pflaum, S. Hirschmann, W. Zhuang, F. Jaiser, U. Asawapirom, J. P. Rape, U. Scherf, D. Neher, *Adv. Funct. Mater.* **2004**, *14*, 757–764.
- [23] J.-Y. Lee, C.-J. Lin, C.-T. Lo, J.-C. Tsai, W.-C. Chen, *Macromolecules* **2013**, *46*, 3005–3014.
- [24] X. N. Zhang, L. J. Richter, D. M. DeLongchamp, R. J. Kline, M. R. Hammond, I. McCulloch, M. Heeney, R. S. Ashraf, J. N. Smith, T. D. Anthopoulos, B. Schroeder, Y. H. Geerts, D. A. Fischer, M. F. Toney, *J. Am. Chem. Soc.* **2011**, *133*, 15073–15084.

Manuscript received: April 19, 2018

Accepted manuscript online: May 7, 2018

Version of record online: May 23, 2018